



Emergent constraint on Arctic Ocean acidification in the twenty-first century

Jens Terhaar, Lester Kwiatkowski, Laurent Bopp

► To cite this version:

Jens Terhaar, Lester Kwiatkowski, Laurent Bopp. Emergent constraint on Arctic Ocean acidification in the twenty-first century. *Nature*, 2020, 582 (7812), pp.379-383. 10.1038/s41586-020-2360-3 . hal-02884111

HAL Id: hal-02884111

<https://hal.science/hal-02884111>

Submitted on 10 Nov 2020

HAL is a multi-disciplinary open access archive for the deposit and dissemination of scientific research documents, whether they are published or not. The documents may come from teaching and research institutions in France or abroad, or from public or private research centers.

L'archive ouverte pluridisciplinaire **HAL**, est destinée au dépôt et à la diffusion de documents scientifiques de niveau recherche, publiés ou non, émanant des établissements d'enseignement et de recherche français ou étrangers, des laboratoires publics ou privés.

Emergent constraint on Arctic Ocean acidification in the twenty-first century

Jens Terhaar^{1,2,3*}, Lester Kwiatkowski^{1,4}, Laurent Bopp¹

¹ LMD/IPSL, Ecole Normale Supérieure/PSL Université, CNRS, Ecole Polytechnique, Sorbonne
Université, Paris, France

² Climate and Environmental Physics, Physics Institute, University of Bern, Switzerland

³ Oeschger Center for Climate Change Research, University of Bern, Switzerland

⁴ LOCEAN/IPSL, Sorbonne Université, CNRS, IRD, MNHN, Paris, France

***Jens Terhaar**

Climate and Environmental Physics, Physics Institute

University of Bern

Sidlerstrasse 5

3012 Bern

Switzerland

jens.terhaar@climate.unibe.ch

The ongoing uptake of anthropogenic carbon by the ocean leads to ocean acidification, a process that results in a reduction in pH and the saturation state of biogenic calcium carbonate minerals ($\Omega_{\text{calc/arag}}$)^{1,2}. Due to naturally low $\Omega_{\text{calc/arag}}$ ^{2,3}, the Arctic Ocean is considered the most susceptible region to future acidification and associated ecosystem impacts^{4,5,6,7}. However, the magnitude of projected twenty-first century acidification differs strongly across Earth System Models (ESMs)⁸. Here we identify an emergent multi-model relationship between the simulated present-day density of Arctic Ocean surface waters, used as a proxy for Arctic deep-water formation, and projections of the anthropogenic carbon inventory and coincident acidification. Applying observations of sea surface density, we constrain the end of twenty-first century Arctic Ocean anthropogenic carbon inventory to 9.0 ± 1.6 Pg C and basin-averaged Ω_{arag} and Ω_{calc} to 0.76 ± 0.06 and 1.19 ± 0.09 respectively, under the RCP 8.5 climate scenario. Our results indicate greater regional anthropogenic carbon storage and ocean acidification than previously projected^{3,8} and increase the probability that large parts of the mesopelagic Arctic Ocean will be undersaturated with respect to calcite by the end of the century. This increased rate of Arctic Ocean acidification combined with rapidly changing physical and biogeochemical Arctic conditions^{9,10,11}, is likely to exacerbate the impact of climate change on vulnerable Arctic marine ecosystems.

While the uptake of atmospheric carbon by the ocean mitigates climate change, it also dramatically influences marine chemistry, decreasing pH and carbonate ion concentrations $[\text{CO}_3^{2-}]$ and increasing concentrations of aqueous carbon dioxide and bicarbonate ions $[\text{HCO}_3^-]$ ^{1,2}. These changes in seawater chemistry, collectively known as ocean acidification, have been shown to negatively impact wide-ranging marine organisms including molluscs, crustaceans, echinoderms, cnidarians and teleost fish^{4,5,6,7}. Calcifying marine organisms are particularly sensitive to ocean acidification, which can impair their growth, reproduction and survival^{2,4,12}. The thermodynamic stability of calcium carbonate is described by the calcium carbonate saturation state ($\Omega = [\text{Ca}^{2+}][\text{CO}_3^{2-}]/K_{\text{sp}}$), with K_{sp} representing the relevant CaCO_3 solubility product, and Ω_{calc} and Ω_{arag} representing the saturation state of the stable calcite and metastable aragonite mineral forms, respectively. Ocean acidification acts to reduce Ω by reducing carbonate ion concentrations. Studies have shown that as Ω decreases, calcification rates at both the organism^{12,13,14} and community-level¹⁵ typically decline. In addition, the corrosion of pure mineral forms is actively promoted under exposure to undersaturated conditions ($\Omega < 1$).

The Arctic represents the global region projected to experience the most severe climate change, with polar amplification causing a projected end-of-century surface temperature increase of up to 8.3 ± 1.9 °C¹⁰ and loss of summer sea-ice¹¹. The same is true for the Arctic Ocean, where low temperatures and consequently the high solubility of CO_2 , result in naturally low pH and Ω ^{2,3}. Given this natural state and the amplifying effect of climate change¹⁶, the

Arctic Ocean is projected to experience the lowest pH and Ω conditions in the coming decades³, as well as dramatic changes in the temporal variability of marine chemistry⁹.

Projections by ESMs under the high-emissions Representative Concentration Pathway 8.5 (RCP8.5)¹⁷ suggest that the entire Arctic Ocean will be undersaturated with respect to aragonite ($\Omega_{\text{arag}} < 1$) by the end of the twenty-first century (Fig. 1), while basin-wide calcite undersaturation ($\Omega_{\text{calc}} < 1$) is not expected to occur this century^{3,8,18} (Extended Data Figure 1). Projected changes in ocean chemistry are predominantly confined to the upper 2500 m of the water column, with large model uncertainties persisting with regard to the end-of-century anthropogenic carbon inventory (2.9-13.0 Pg C)¹⁹, and the associated average Ω_{arag} (0.66-0.95) and Ω_{calc} (1.02-1.49)⁸. Although projection uncertainties are limited in the surface ocean²⁰, they are highly pronounced at depth (Fig. 1 and Extended Data Figure 1) and complicate assessments of likely impacts on vulnerable marine ecosystems⁷.

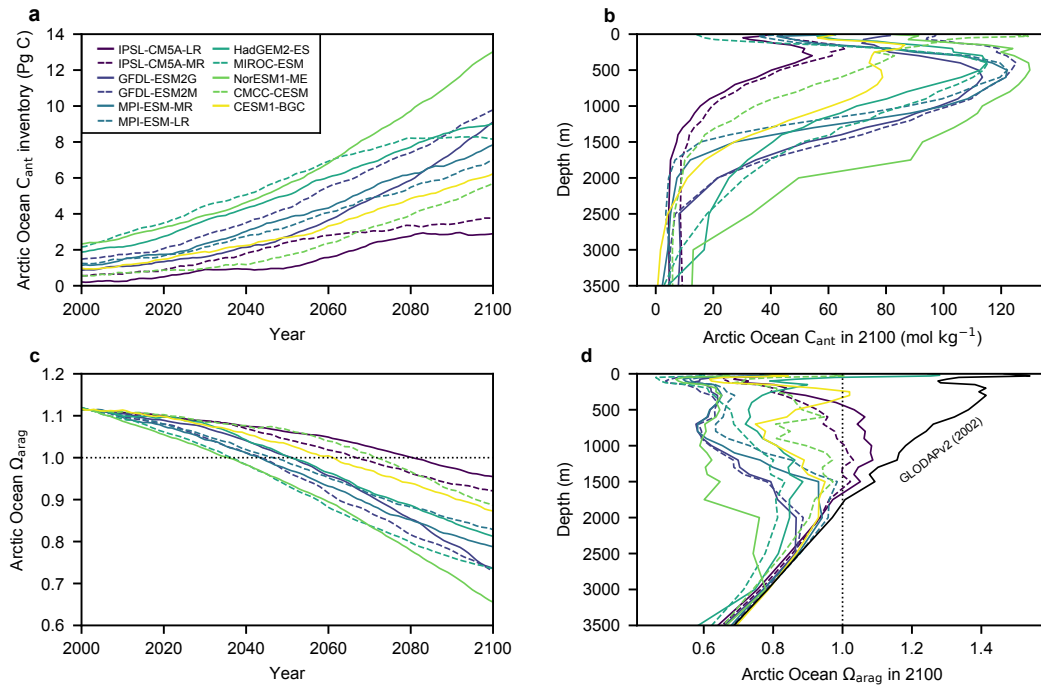


Fig. 1. Projections of Arctic Ocean anthropogenic carbon and aragonite saturation state. **a**, ESM projections of the twenty-first century Arctic Ocean anthropogenic carbon (C_{ant}) inventory and **c**, basin-averaged Ω_{arag} . Vertical profiles of **b**, basin-averaged anthropogenic carbon and **d**, Ω_{arag} in 2100 for the 11 ESMs. The GLODAPv2²⁴ observational profile of Ω_{arag} for 2002 is marked as a black line in **d**. Arctic Ocean boundaries are the Fram Strait, the Barents Sea Opening, the Bering Strait and the Canadian Arctic Archipelago.

To reduce Arctic Ocean projection uncertainties associated with the anthropogenic carbon inventory and concurrent acidification, here we utilise the recent approach of emergent constraints^{11,21,22,23}. In order to constrain future ESM projection uncertainties, emergent constraints relate long-timescale climate sensitivities and impacts to observable properties, such as short-timescale climate variability or trends, across ESM ensembles. Emergent

constraints have previously been used to reduce the uncertainty, amongst other climate projections, associated with Arctic summer sea ice¹¹, equilibrium climate sensitivity²² and impacts on marine primary production²¹.

Here we show that across an ensemble of 11 ESMs (Table S1) there is a consistent relationship between present-day Arctic Ocean maximum sea surface water density, the projected end-of-century Arctic Ocean anthropogenic carbon inventory and the extent of ocean acidification under RCP8.5 (Fig. 2, 3). All models performed simulations as part of the Coupled Model Intercomparison Project Phase 5 (CMIP5). Present-day (1986-2005) maximum sea surface density was calculated, for each model, as the mean of the 95th percentile of monthly surface water densities in the Arctic. Across all models, these maximum density waters are primarily located in the Barents Sea (Extended Data Figure 2). The anthropogenic carbon inventory was calculated as the difference in integrated Arctic Ocean dissolved inorganic carbon between RCP8.5 simulations and the respective pre-industrial control simulation of each model. While projections of variables associated with ocean acidification ($\Omega_{\text{calc/arag}}$, pH and $p\text{CO}_2$) were calculated from model outputs of total alkalinity, dissolved inorganic carbon, temperature, salinity, total dissolved inorganic phosphorus and silicon and bias-corrected using GLODAPv2²⁴ (see Methods).

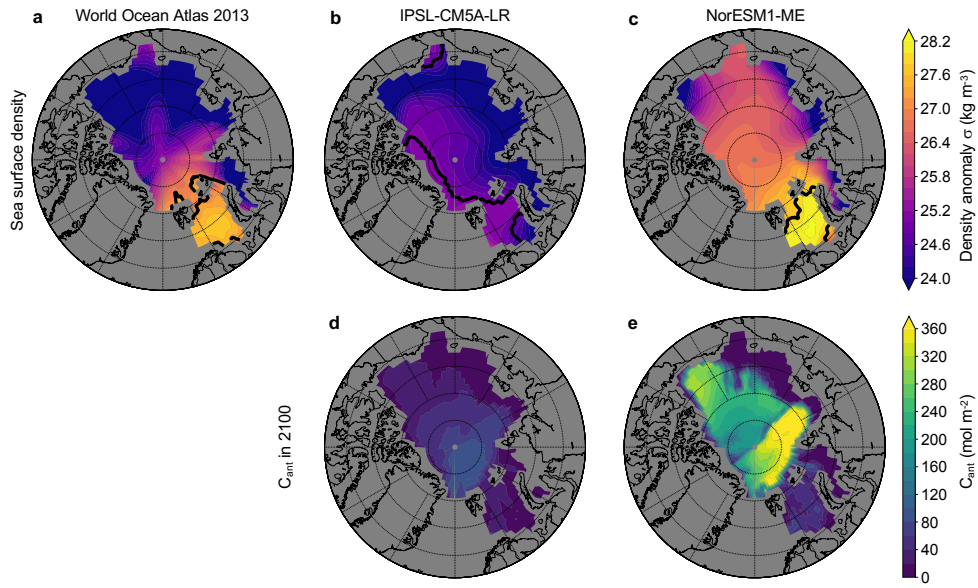


Fig. 2. Arctic Ocean surface water density and the anthropogenic carbon inventory. **a**, Present-day annual-mean sea surface density from World Ocean Atlas 2013²⁵ and the **b**, IPSL-CM5A-LR and **c**, NorESM1-ME models. Contours delineate regions that contribute to the maximum surface density as defined by the 95th percentile densities. Vertically integrated anthropogenic carbon (C_{ant}) projections in 2100 for the **d**, IPSL-CM5A-LR and **e**, NorESM1-ME models. IPSL-CM5A-LR represents the ensemble minimum for both present-day maximum sea surface density ($1025.67 \text{ kg m}^{-3}$) and projected C_{ant} inventory in 2100 (2.9 Pg C), while NorESM1-ME is the ensemble maximum ($1028.24 \text{ kg m}^{-3}$ and 13.0 Pg C). The maximum sea surface density from WOA 2013 is $1027.85 \text{ kg m}^{-3}$

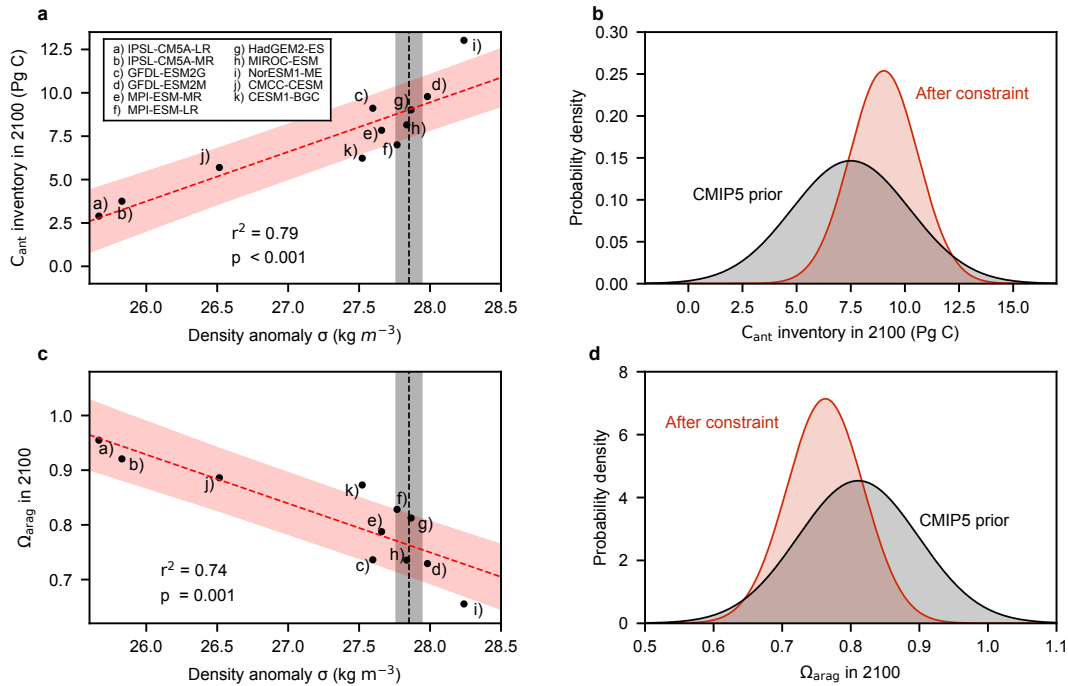


Fig. 3. Emergent constraints on the projected anthropogenic carbon inventory and future acidification. **a**, The projected Arctic Ocean anthropogenic carbon inventory and **c**, basin-averaged Ω_{arag} in 2100 against present-day maximum sea surface density (95th percentile waters) for the ESM ensemble (black dots). Linear regression fits (red dashed lines) and the associated 68 % prediction intervals are shown, as are data-based estimates of present-day maximum sea surface density (black dashed lines) with the associated standard deviation (black shaded area). Probability density functions for the end-of-century **b**, Arctic Ocean anthropogenic carbon inventory and **d**, basin-averaged Ω_{arag} , before (black) and after (red) the emergent constraint is applied.

ESMs such as IPSL-CM5A-LR, which simulate lower than observed present-day Arctic Ocean maximum surface densities, a proxy for Arctic deep-water formation (Extended Data Figure 3), typically project lower end-of-century anthropogenic carbon inventories under RCP8.5 than models such as NorESM1-ME, which simulate higher densities (Fig. 2). This emergent relationship across the ESM ensemble is consistent at the scale of the Arctic Ocean basin, with present-day maximum surface density exhibiting a strong relationship with end-of-century depth integrated anthropogenic carbon inventories ($r^2=0.79$, $P < 0.001$; Fig. 3). Given the dominance of anthropogenic carbon uptake in driving ocean acidification (Extended Data Figure 4), models with higher maximum sea surface density also exhibit stronger twenty-first century reductions in basin-average Ω_{arag} ($r^2=0.74$, $P = 0.001$; Fig. 3), Ω_{calc} ($r^2=0.74$, $P = 0.001$; Extended Data Figure 1) and pH ($r^2=0.77$, $P < 0.001$; Extended Data Figure 1). Observations of sea surface density²⁵ were then used in combination with these multi-model relationships, to provide emergent constraints on projections of Arctic Ocean anthropogenic carbon storage, and concomitant acidification. Potential alternative constraints, such as present-day seasonal sea ice extent, were found to be non-indicative of future Arctic Ocean anthropogenic carbon and acidification across the ESM ensemble (Extended Data Figure 3).

Our emergent constraint increases projections of the end-of-century Arctic Ocean anthropogenic carbon inventory from 7.5 ± 2.7 Pg C (CMIP5 multi-model mean) to 9.0 ± 1.6 Pg C, with a 41 % reduction in uncertainty (Fig. 3). Similarly, average end-of-century Ω_{arag} and Ω_{calc} are reduced from 0.81 ± 0.09 to 0.76 ± 0.06 and from 1.27 ± 0.14 to 1.19 ± 0.09 , respectively

(Fig. 3, Extended Data Figure 1). As such, the low bias of maximum sea surface density in 8 of 11
ESMs is indicative of an underestimation of projected anthropogenic carbon storage and
therefore future Arctic Ocean acidification in the CMIP5 multi-model mean.

The mechanisms underpinning the relationship between maximum surface densities and
anthropogenic carbon uptake are intrinsically related to Arctic Ocean circulation and dynamics.
The majority of intermediate and deep Arctic waters and the anthropogenic carbon they carry
are of Atlantic origin^{26,27}. The dominant net influx of anthropogenic carbon from the Atlantic
into the Arctic Ocean is through the Barents Sea Opening, as indicated by both data-based
estimates²⁸ ($41 \pm 8 \text{ Tg C yr}^{-1}$) and ocean carbon cycle models (21-48 Tg C yr^{-1} ; Table S2). This
inflowing water is seasonally cooled in the Barents Sea via surface heat exchange and enriched
in salinity via brine rejection during the formation of sea ice^{29,30}. Consequently, during winter,
seawater density increases and water masses sink into the interior Arctic Ocean, mainly via the
St Anna Trough, where they supply most intermediate and deep waters^{26,27}. As such, the
present-day ability of ESMs to simulate the maximum surface densities that occur in the
Barents Sea, is highly indicative of their capacity to transport future anthropogenic carbon into
the Arctic interior.

These mechanisms were further explored in historical (1870-2012) simulations of an ocean-only
carbon-cycle model (NEMO-PISCES), performed at three spatial resolutions¹⁹. These simulations
confirm the importance of Atlantic waters that flow into the Barents Sea, in determining net

changes in the Arctic Ocean anthropogenic carbon inventory (Table S2). They further show that across model spatial resolutions there is a strong positive relationship ($r^2=0.98$, $P = 0.08$; Fig. S1) between maximum surface density and the historical change in Arctic Ocean anthropogenic carbon inventory (Fig. S2). One of the principal drivers of the CMIP5 emergent relationship therefore appears to be variable ESM resolution and associated difficulties in resolving the transport of anthropogenic carbon into the Arctic basin at low resolutions¹⁹. Indeed, CMIP5 ESMs with higher Arctic Ocean resolution typically project greater end-of-century anthropogenic carbon inventories ($r^2=0.44$, $P = 0.03$; Extended Data Figure 3).

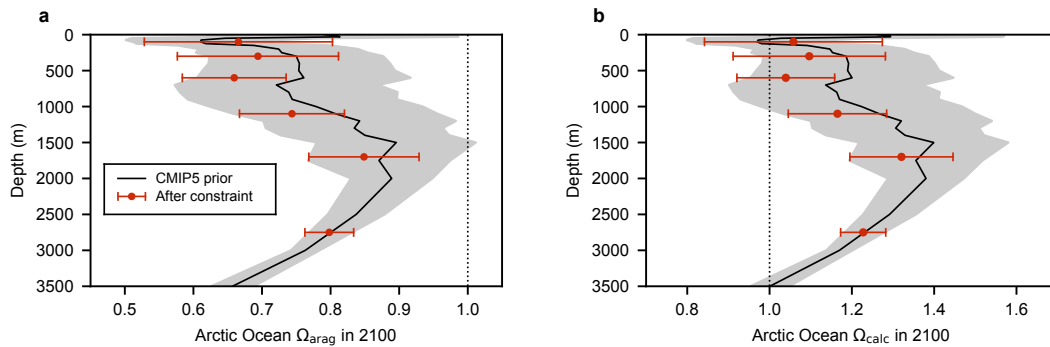


Fig. 4. Constrained end-of century Arctic Ocean vertical profiles of $\Omega_{\text{calc/arag}}$. Multi-model mean vertical profiles of basin-averaged **a**, Ω_{arag} and **b**, Ω_{calc} in 2100 (black lines) with the associated standard deviation ($n=11$; grey shading). Constrained mean estimates of Ω_{arag} and Ω_{calc} (red dots) are shown for six different depth layers (0-200 m, 200-400 m, 400-800 m, 800-1400 m, 1400-2000 m, 2000 m - bottom). The constrained estimates are shown at the mid-point of each layer, with error bars representing \pm one standard deviation.

Extending the emergent constraint approach from the entire Arctic basin to multiple vertical depth integrals, we reduce uncertainties associated with projections of changing vertical profiles of $\Omega_{\text{calc/arag}}$ (Fig. 4, Extended Data Figures 5, 6), pH and $p\text{CO}_2$ (Extended Data Figures 7, 8). Basin-wide emergent constraints on twenty-first century acidification are shown to be predominantly driven by subsurface waters between 400 and 1400 m, with the strongest multi-model relationship between present-day maximum surface density and end-of-century $\Omega_{\text{calc/arag}}$ found between 400 and 800 m ($r^2 = 0.84$, $P < 0.001$; Extended Data Figures 5, 6). In these mesopelagic waters, end-of-century Ω_{arag} is reduced from a CMIP5 multi-model mean of 0.75 ± 0.15 to 0.66 ± 0.08 , with end-of-century Ω_{calc} reduced from 1.18 ± 0.23 to 1.04 ± 0.12 . A consequence of our constrained vertical profiles of marine chemistry is that the lowest average end-of-century $\Omega_{\text{calc/arag}}$ will likely not occur in Arctic Ocean surface waters, as previously expected^{3,8}, but between 400-800 m (Fig. 4). In these mesopelagic waters, the probability of end-of-century $\Omega_{\text{calc}} < 1$ and $\Omega_{\text{arag}} < 0.75$ is increased from 23% and 51% respectively in the CMIP5 prior to 37% and 88% respectively after the constraint is applied (Extended Data Table 1).

In the upper Arctic Ocean (0-200 m), present-day maximum surface density exhibits limited relationship with end-of-century $\Omega_{\text{calc/arag}}$ across the models (Extended Data Figures 5, 6) and emergent constraints offer no reduction in projection uncertainties (Fig. 4). This is to be expected in waters where deep-water formation has little impact on marine chemistry. Similarly, below 2000 m where there is limited change in the anthropogenic carbon inventory

and associated marine chemistry this century (Fig. 1, Extended Data Figure 1), there is no relationship between present-day maximum surface density and end-of-century $\Omega_{\text{calc/arag}}$ (Extended Data Figures 5, 6).

The constrained estimates of greater twenty-first century Arctic Ocean acidification presented here, have major implications for sensitive Arctic marine ecosystems already exposed to multiple climatic stressors. Enhanced subsurface acidification is likely to have negative consequences on organisms that both permanently inhabit the mesopelagic and those that utilise it as part of seasonal or diel vertical migrations³¹. The suitable habitat available to keystone species such as the aragonitic pteropod *Limacina helicina* is likely to decline to a greater extent than previously anticipated given its sensitivity to Ω_{arag} ³², with negative consequences for dependent pelagic food webs^{33,34,35}. Meanwhile, undersaturation with respect to calcite is likely to have major consequences for calcite forming Arctic coccolithophores³⁶ and foraminifera³⁷. Finally, our estimates of higher end-of century Arctic Ocean $p\text{CO}_2$, which increases from $1070 \pm 239 \mu\text{atm}$ at depths of 400-800 m to $1216 \pm 121 \mu\text{atm}$ under the constraint (Extended Data Figure 8), is likely to negatively affect the growth, survival³⁸ and behaviour^{39,40} of ecologically important fish such as polar cod.

229 **References**

- 230 1. Haugan, P. M. & Drange, H. Effects of CO₂ on the ocean environment. *Energy Convers.*
231 *Mgmt* **37**, 1019–1022 (1996).
- 232 2. Orr, J. C. et al. Anthropogenic ocean acidification over the twenty-first century and its
233 impact on calcifying organisms. *Nature* **437**, 681–686 (2005).
- 234 3. Steinacher, M., Joos, F., Frolicher, T. L., Plattner, G. K. & Doney, S. C. Imminent ocean
235 acidification in the Arctic projected with the NCAR global coupled carbon cycle-climate model.
236 *Biogeosciences* **6**, 515–533 (2009).
- 237 4. Fabry, V. J., McClintock, J. B., Mathis, J. T. & Grebmeier, J. M. Ocean acidification at high
238 latitudes: The bellweather. *Oceanography* **22**, 160–171 (2009).
- 239 5. Gattuso, J.-P. & Hansson, L. *Ocean Acidification* (Oxford Univ. Press, 2011).
- 240 6. Riebesell U, Gattuso JP, Thingstad TF, Middelburg JJ. Preface “Arctic ocean acidification:
241 pelagic ecosystem and biogeochemical responses during a mesocosm study”. *Biogeosciences*
242 **10**(8), 5619–5626 (2013).
- 243 7. AMAP, 2018. AMAP Assessment 2018: Arctic Ocean Acidification. Arctic Monitoring and
244 Assessment Programme (AMAP), Tromsø, Norway. vi+187pp
- 245 8. Steiner, N. S., Christian, J. R., Six, K. D., Yamamoto, A., & Yamamoto-Kawai, M. Future
246 ocean acidification in the Canada Basin and surrounding Arctic Ocean from CMIP5 earth system
247 models. *Journal of Geophysical Research: Oceans* **119**(1), 332–347 (2014).

- 248 9. Kwiatkowski, L. & Orr, J.C. Diverging seasonal extremes for ocean acidification during
249 the twenty-first century. *Nature Climate Change* **8**(2), 141 (2018)
- 250 10. Collins, M. et al. in *Climate Change 2013: The Physical Science Basis* (eds Stocker, T. F. et
251 al.) 1029–1136 (IPCC, Cambridge Univ. Press, 2013).
- 252 11. Boé, J., Hall, A. & Qu, X. September sea ice cover in the Arctic Ocean projected to vanish
253 by 2100. *Nature Geosci.* **2**, 341–343 (2009).
- 254 12. Kroeker, K. J., Kordas, R. L., Crim, R. N. & Singh, G. G. Meta-analysis reveals negative yet
255 variable effects of ocean acidification on marine organisms. *Ecol. Lett.* **13**, 1419–1434 (2010).
- 256 13. Langdon, C. & Atkinson, M. Effect of elevated $p\text{CO}_2$ on photosynthesis and calcification
257 of corals and interactions with seasonal change in temperature/irradiance and nutrient
258 enrichment. *J. Geophys. Res.* **110**, C09S07 (2005).
- 259 14. Bednaršek, N., Tarling, G. A., Bakker, D. C., Fielding, S. & Feely, R. A. Dissolution
260 dominating calcification process in polar pteropods close to the point of aragonite
261 undersaturation. *PLoS ONE* **9**(10), e109183 (2014).
- 262 15. Albright, R. et al. Reversal of ocean acidification enhances net coral reef calcification.
263 *Nature* **531**, 362–365 (2016).
- 264 16. Yamamoto-Kawai, M., McLaughlin, F. A., Carmack, E. C., Nishino, S. & Shimada, K.
265 Aragonite undersaturation in the Arctic Ocean: Effects of ocean acidification and sea ice melt.
266 *Science* **326**, 1098–1100 (2009).

- 267 17. Riahi, K. et al. RCP 8.5—A scenario of comparatively high greenhouse gas emissions.
268 *Clim. Change* **109**, 33–57 (2011).
- 269 18. Feely, R. A., Doney, S. C. & Cooley, S. R. Ocean acidification: Present conditions and
270 future changes in a high-CO₂ world. *Oceanography* **22**, 36–47 (2009).
- 271 19. Terhaar, J., Orr, J. C., Gehlen, M., Ethé, C., and Bopp, L. Model constraints on the
272 anthropogenic carbon budget of the Arctic Ocean. *Biogeosciences* **16**, 2343–2367 (2019).
- 273 20. Frolicher, T. L., Rodgers, K., Stock, C. & Cheung, W. W. L. Sources of uncertainties in 21st
274 century projections of potential ocean ecosystem stressors. *Global Biogeochem. Cycles* **30**,
275 1224–1243 (2016).
- 276 21. Kwiatkowski, L. et al. Emergent constraints on projections of declining primary
277 production in the tropical oceans. *Nat. Clim. Chang.* **7**, 355–358 (2017).
- 278 22. Cox, P. et al. Sensitivity of tropical carbon to climate change constrained by carbon
279 dioxide variability. *Nature* **494**, 341–344 (2013)
- 280 23. Eyring, V. et al. Taking climate model evaluation to the next level. *Nat. Clim. Chang.* **9**,
281 102–110 (2019).
- 282 24. Lauvset, S. K. et al. A new global interior ocean mapped climatology: the 1°×1° GLODAP
283 version 2. *Earth Syst. Sci. Data* **8**, 325–340 (2016).
- 284 25. Boyer, T. P. et al. *World Ocean Database 2013* (Silver Spring, accessed March 2019).
- 285 26. Rudels, B., Jones, E. P., Anderson, L. G., & Kattner, G. On the intermediate depth waters

286 of the Arctic Ocean. *The polar oceans and their role in shaping the global environment*, **85**, 33-
 287 46 (1994).

288 27. Rudels, B., Muench, R. D., Gunn, J., Schauer, U., & Friedrich, H. J. Evolution of the Arctic
 289 Ocean boundary current north of the Siberian shelves. *J. Marine Syst.*, **25**(1) . (2001). 77-99.

290 28. Jeansson, E. et al. The Nordic Seas carbon budget: Sources, sinks, and uncertainties.
 291 *Global Biogeochem, Cy.*, **25**(4). (2011)

292 29. Midttun, Lars. "Formation of dense bottom water in the Barents Sea." *Deep Sea Res.*
 293 **32**.10, 1233-1241 (1985)

294 30. Smedsrud, L. H. et al. The role of the Barents Sea in the Arctic climate system. *Rev.*
 295 *Geophys.* **51**, 415–449 (2013).

296 31. Berge, J. et al. In the dark: A review of ecosystem processes during polar night. *Prog.*
 297 *Oceanogr.* **139**, 258–271 (2015).

298 32. Comeau, S., Jeffree, R., Teyssie, J. L. & Gattuso, J. P. Response of the Arctic pteropod
 299 *Limacina helicina* to projected future environmental conditions. *PLoS ONE* **5**, e11362 (2010).

300 33. Hunt, B. P. V. et al. Pteropods in Southern Ocean ecosystems. *Prog. Oceanogr.* **78**, 193–
 301 221 (2008).

302 34. Armstrong, J. L. et al. Distribution, size, and interannual, seasonal and diel food habits of
 303 northern Gulf of Alaska juvenile pink salmon, *Oncorhynchus gorbuscha*. *Deep-Sea Res. Pt. II* **52**,
 304 247–265 (2005).

- 305 35. Karnovsky, N. J., Hobson, K. A., Iverson, S., & Hunt Jr, G. L. Seasonal changes in diets of
306 seabirds in the North Water Polynya: a multiple-indicator approach. *Mar. Ecol. Prog. Ser.*, **357**,
307 291–299 (2008).
- 308 36. Kottmeier, D. M., Rokitta, S. D., & Rost, B. H^+ -driven increase in CO_2 uptake and decrease
309 in HCO_3^- uptake explain coccolithophores' acclimation responses to ocean acidification. *Limnol.*
310 *Oceanogr.* **61**, 2045–2057 (2016)
- 311 37. Davis, C. V. et al. Ocean acidification compromises a planktic calcifier with implications
312 for global carbon cycling. *Sci. Rep.* **7**, 2225 (2017)
- 313 38. Frommel, A. Y. et al. Severe tissue damage in Atlantic cod larvae under increasing ocean
314 acidification. *Nature Clim. Change* **2**, 42–46 (2012).
- 315 39. Schmidt, M. et al. Differences in neurochemical profiles of two gadid species under
316 ocean warming and acidification. *Front. Zool.* **14**, 49 (2017).
- 317 40. Kunz, K. et al. Aerobic capacities and swimming performance of polar cod (*Boreogadus*
318 *saida*; lepechin) under ocean acidification and warming conditions. *J. Exp. Biol.* **221** (2018)

319

Methods

Earth System Models

In the ensemble of 11 Coupled Model Intercomparison Project Phase 5 (CMIP5) ESMs (Table S1) utilised, all included coupled ocean biogeochemistry schemes and have been extensively applied within the context of both climate and ocean biogeochemical projections^{8,9,21}. A single ensemble member was utilised for each ESM. Prognostic annual model output fields of dissolved inorganic carbon, total alkalinity, dissolved inorganic phosphorus and silicon, temperature, and salinity were taken across all vertical depth levels in the Arctic Ocean, limited by the Fram Strait, the Barents Sea Opening, the Bering Strait and the Canadian Arctic Archipelago^{19,41}. Monthly sea surface density outputs were taken over the same domain. All output fields were regridded on a regular 1°×1° grid to facilitate multi-model analysis.

The anthropogenic carbon inventory was calculated as the difference between dissolved inorganic carbon in historical (1850-2005) simulations merged with RCP8.5 (2006-2100) and the concurrent pre-industrial control (piControl) simulations. As such, any model drift in deep-ocean dissolved inorganic carbon was directly accounted for. Across all models, the simulated present-day (2005) Arctic Ocean anthropogenic carbon inventory (0.2-2.4 Pg C) is below the data-based estimate of 2.5-3.3 Pg C⁴².

All carbonate chemistry variables were calculated offline from dissolved inorganic carbon, total alkalinity, temperature, salinity and where available, dissolved inorganic phosphorus and silicon, over 1850-2100 using mocsy2.0⁴³ and the equilibrium constants recommended for best

practices⁴⁴. To account for carbonate chemistry biases in the present-day mean state of the
ESMs⁸, model anomalies of all input variables relative to 2002 were combined with the data-
based GLODAPv2 observational product²⁴ which is normalised to the year 2002. Model
anomalies were corrected for potential model drift using concurrent piControl simulations. All
grid cells with GLODAPv2 observational coverage (~65 % of Arctic Ocean volume) were utilised.
Basin-wide averages of Ω_{arag} , Ω_{calc} , pH and $p\text{CO}_2$ were weighted based on grid cell volumes.

The Arctic Ocean present-day maximum sea surface density was calculated for each ESM from
1986-2005 monthly sea surface density climatologies, constructed from temperature and
salinity outputs. Maximum present-day sea surface density was defined as the mean density of
the densest 5 % of Arctic surface waters (95th percentile waters) throughout the climatological
year. Maximum present-day sea surface density consistently occurs in the Barents Sea, across
both observations and the ESM ensemble. Given the importance of the Barents Sea in supplying
intermediate and deep Arctic waters^{26,27,29,30}, maximum sea surface density, as defined, is
indicative of the bowl of ventilated Arctic waters. Across all models, the volume of Arctic Ocean
waters that are lighter than the maximum sea surface density increases with the maximum sea
surface density ($r^2 = 0.59$, $P=0.006$; Extended Data Figure 3).

In addition to sea surface density, alternative potential constraints on the projected Arctic
Ocean anthropogenic carbon inventory and associated acidification were assessed. The
representation of Arctic sea ice extent⁴⁵ and intermediate North Atlantic water masses⁴⁶ varies
substantially across the CMIP5 ensemble. However, both present-day sea-ice extent (Extended
Data Figure 3) and the properties of North Atlantic water masses were found to be non-

indicative of projected Arctic Ocean carbon uptake and associated acidification across the model ensemble.

An assessment of the potential for model internal variability to influence the Arctic Ocean emergent constraint approach is provided in the supplementary material. Utilising four ensemble members of the IPSL-CM5A-LR model, the internal variability of present-day sea surface density and projected anthropogenic carbon inventory is shown to be highly limited compared to the differences across the CMIP5 models (Extended Data Figure 9).

Ocean-only simulations

Hindcast ocean-biogeochemical simulations of the NEMO-PISCES model⁴⁷ that have been previously published¹⁹ are used in this study to explore the mechanisms behind the identified Arctic Ocean emergent constraint. The model is run at a nominal resolution of 0.5° from 1870 to 1958 and at three different nominal horizontal resolutions from 1958 to 2012: 2° (ORCA2), 0.5° (ORCA05), and 0.25° (ORCA025). All three model configurations are forced with the DRAKKAR historical reanalysis forcing dataset⁴⁸ and therefore only differ in horizontal resolution and the associated diffusion scheme and coefficients.

Observational constraints

Observational sea surface density constraints were derived from the World Ocean Atlas 2013 temperature and salinity climatologies²⁵. The maximum Arctic Ocean sea surface density was then calculated in the same manner as for the ESM ensemble.

The uncertainty associated with Arctic Ocean maximum sea surface density observational constraints was estimated using standard propagation of uncertainty and combining (1) the published standard deviations of sea surface temperature and salinity for each grid cell and each month in WOA2013 to derive standard deviations for sea surface density, and (2) the standard deviation obtained when computing the weighted mean of 95th percentile density waters.

Arctic Ocean salinity in World Ocean Atlas 2013 was recently evaluated against available in-situ data⁴⁹. This comparison suggests that salinity observations in the World Ocean Atlas may have a small negative bias in the Barents Sea that may contribute to a negative density bias. Corroboration and correction of such a bias would, if anything, result in a minor increase in our constrained estimates of projected Arctic Ocean anthropogenic carbon and associated acidification.

Probability density functions of anthropogenic carbon and ocean acidification

Probability density functions (PDFs) of anthropogenic carbon storage and basin-averaged Ω_{arag} , Ω_{calc} and pH in 2100 were calculated for the unconstrained (prior) CMIP5 ensemble and the

401 emergent constraints. The prior PDF was derived assuming all models were equally likely and
402 sampled from a Gaussian distribution. The constrained PDFs were calculated as the normalised
403 product of the conditional PDF of the emergent relationship and the PDF of the observational
404 constraint following previously established methodologies^{21,22,50}.

405

406

References (Methods)

41. Bates, N. R. & Mathis, J. T. The Arctic Ocean marine carbon cycle: Evaluation of air-sea CO₂ exchanges, ocean acidification impacts and potential feedbacks. *Biogeosciences* **6**, 2433–2459 (2009).
42. Tanhua, T. et al. Ventilation of the Arctic Ocean: mean ages and inventories of anthropogenic CO₂ and CFC-11. *J. Geophys. Res.* **114** (2009).
43. Orr, J. C. & Epitalon, J.-M. Improved routines to model the ocean carbonate system: mocsy 2.0. *Geosci. Model Dev.* **8**, 485–499 (2015).
44. Dickson, A. G., Sabine, C. L. & Christian, J. R. (eds) *Guide to Best Practices For Ocean CO₂ Measurements* 191 (PICES Special Publication 3, 2007).
45. Shu, Q., Song, Z. & Qiao, F. Assessment of sea ice simulations in the CMIP5 models. *Cryosphere* **9**, 399–409 (2015).
46. Shu, Q., Wang, Q., Su, J., Li, X., & Qiao, F. Assessment of the Atlantic water layer in the Arctic Ocean in CMIP5 climate models. *Clim. Dyn.* **53** 5279–5291 (2019).
47. Aumont, O. & Bopp, L. Globalizing results from ocean in situ iron fertilization studies. *Glob. Biogeochem. Cycles* **20**, GB2017 (2006).
48. Brodeau, L., Barnier, B., Treguier, A. M., Penduff, T. & Gulev, S. An ERA40-based atmospheric forcing for global ocean circulation models. *Ocean Model.* **31**, 88–104 (2010).
49. Xie, J., Raj, R. P., Bertino, L., Samuelsen, A., & Wakamatsu, T. Evaluation of Arctic Ocean surface salinities from SMOS and two CMEMS reanalyses against in situ data sets. *Ocean Sci.* **15**,

427 1191–1206 (2019).

428 50. Wenzel, S., Cox, P. M., Eyring, V. & Friedlingstein, P. Emergent constraints on climate-
429 carbon cycle feedbacks in the CMIP5 Earth system models. *J. Geophys. Res. Biogeosciences* **119**,
430 2013JG002591 (2014).

431

432

433

Acknowledgements

This study was funded by the H2020 C-CASCADES grant (ref 643052), the H2020 CRESCENDO grant (ref 641816), the H2020 4C grant (ref 821003), the Agence Nationale de la Recherche grant ANR-18-ERC2-0001-01 (CONVINCE), the MTES/FRB Acidoscope project and the ENS-Chanel research chair. We acknowledge the World Climate Research Programme's Working Group on Coupled Modelling, which is responsible for CMIP. For CMIP the US Department of Energy's Program for Climate Model Diagnosis and Intercomparison provided coordinating support and led the development of software infrastructure in partnership with the Global Organisation for Earth System Science Portals. The authors also thank the IPSL modelling group for the software infrastructure, which facilitated CMIP5 analysis, Jean-Marc Moline, Laurent Brodeau, and Bernard Barnier for developing the DRAKKAR ORCA05 and ORCA025 global configurations of NEMO and Jennifer Simeon, Christian Ethé, Marion Gehlen, and James C. Orr for the implementation of NEMO-PISCES within these configurations.

Author contributions

This study was conceived by all coauthors. J.T. performed the model output analysis and produced the figures, with help from L.K. and L.B. All authors contributed ideas, discussed the results and wrote the manuscript.

Author information

The authors declare no competing financial interests. Correspondence and requests for materials should be addressed to J.T (jens.terhaar@climate.unibe.ch).

Data availability

The Earth system model output used in this study is available via the Earth System Grid Federation (<https://esgf-node.ipsl.upmc.fr/projects/esgf-ipsl/>). Observations from the World Ocean Atlas 2013 (<https://www.nodc.noaa.gov/OC5/woa18/>) and GLODAPv2 (https://www.nodc.noaa.gov/ocads/oceans/GLODAPv2_2019/) are available via the National Oceanic and Atmospheric Administration. Prior to publication, the output of ocean-only NEMO-PISCES simulations is openly accessible on the ODATIS-supported center ‘Sea scientific open data publication’ (<https://doi.org/10.17882/72239>).

Code availability

The Python module ‘statsmodels’ (<https://www.statsmodels.org/stable/index.html>) was used for linear regression and the calculation of prediction intervals. The mocsy2.0 routines were used to calculate the ocean carbonate system variables (<http://ocmip5.ipsl.jussieu.fr/mocsy/>). The Climate Data Operators (CDO) were used for regridding of CMIP5 model output (<https://code.mpimet.mpg.de/projects/cdo/>). The code for the NEMO ocean model version 3.2 is available under CeCILL license online (<http://www.nemo-ocean.eu>).